International Journal of Pharmaceutics 433 (2012) 129–141

Contents lists available at SciVerse ScienceDirect

International Journal of Pharmaceutics

journal homepage: www.elsevier.com/locate/ijpharm

The effect of poly(ethylene glycol) coating on colloidal stability of superparamagnetic iron oxide nanoparticles as potential MRI contrast agent

Afshin Masoudi[a,*], Hamid Reza Madaah Hosseini[a], Mohammad Ali Shokrgozar[b], Reza Ahmadi[a], Mohammad Ali Oghabian[c,d]

[a] Department of Materials Science and Engineering, Sharif University of Technology, Tehran, Iran
[b] National Cell Bank, Pasteur Institute, Tehran, Iran
[c] Department of Medical Physics and Biomedical Engineering, School of Medicine, Tehran University of Medical Sciences, Tehran, Iran
[d] Research Center for Science and Technology in Medicine, Imam Khomeini Hospital Complex, Tehran, Iran

ARTICLE INFO

Article history:
Received 29 January 2012
Received in revised form 13 April 2012
Accepted 21 April 2012
Available online 8 May 2012

Keywords:
Iron oxide nanoparticle
Colloidal stability
Polyethylene glycol
MRI contrast agent

ABSTRACT

Superparamganetic iron oxide-based contrast agents in magnetic resonance imaging (MRI) have offered new possibility for early detection of lymph nodes and their metastases. According to important role of nanoparticle size in biodistribution, magnetite nanoparticles coated with different polyethylene glycol (PEG) concentrations up to 10/1 PEG/iron oxide weight ratio in an ex situ manner. To predict the PEG-coated nanoparticle behavior in biological media, such as blood stream or tissue, colloidal stability evaluation was performed to estimate the coating endurance in different conditions. Accordingly, optical absorbance measurements were conducted in solutions with different values of pH and NaCl concentrations. The results indicated that at neutral pH condition, nanoparticles treated by 3/1 ratio possessed better stability parameters. Investigating at high pH of 10 resulted in superior stability for bare magnetite nanoparticles due to its higher electrophoretic mobility. Coating material was attacked at acidic solutions which cause samples with higher PEG weight ratio to be settled slower. In various ionic strengths of 10^{-5} to 0.1 M, 3/1 ratio samples offered greater resistivity to sedimentation. The nanoparticles were further investigated by exposure to L929 cell and following up the iron uptake within cells. Finally, detection sensitivities in lymph nodes were evaluated. Particle uptake and the most signal reduction for in vivo MRI studies were also obtained by nanoparticles acquiring lower PEG contents that showed better colloidal stability.

1. Introduction

Superparamagnetic iron oxide nanoparticles (SPIONs) present exceptional properties based on their size, surface and magnetic behavior (Mikhaylova et al., 2004; Gupta and Gupta, 2005; Mahmoudi et al., 2011). These peculiar characteristics make SPIONs appropriate candidate in wide range of biomedical and bioengineering applications including cell targeting and separation (Handgretinger et al., 1998; Yang et al., 2008), MR imaging (LaConte et al., 2007; Ma et al., 2008; Patel et al., 2008; Ahmadi et al., 2011; Schweiger et al., 2011), cancer treatment (Ling et al., 2011), hyperthermia (Laurent et al., 2011), gene (Cheong et al., 2009) and drug delivery (Gupta and Wells, 2004). To be satisfactorily utilized in many of these applications it is necessary to achieve aqueous colloidal dispersions of nanoparticles comprising particles with uniform size and properties that remain stable in biological media (Barrera et al., 2009; Chanteau et al., 2009). The main reason of nanoparticle stability originates from thermal motion of sub-micron sized particles of colloids, known as Brownian motion (Abdelwahed et al., 2006). In this phenomena, random collisions of a particle with other particles, molecules of suspending media and container wall cause continuous change of particle path that withstand sedimentation. However, magnetic nanoparticles due to van-der walls and magnetic dipole–dipole attractive forces have tendency to aggregation (Theerdhala et al., 2010) which consequently results in susceptibility to sedimentation via gravitational force (Abdelwahed et al., 2006). So, many methods have been evaluated to stabilize colloidal dispersions on the basis of repulsion interactions toward hindering aforementioned attractive forces (de Vicente et al., 2000; Viota et al., 2005; Di Marco et al., 2007a). These are accomplished by the formation of an electric double layer at the particle surface that creating electrostatic repulsion between the particles, or by encapsulating them with a suitable coating material to obstruct particle–particle contact through steric repulsion (Tadros, 2007). The total interactions which contribute to the colloidal stability of dispersions can be expressed as

* Corresponding author. Tel.: +98 912 1830687; fax: +98 21 66005717.
E-mail address: afshin_masoudi@mehr.sharif.edu (A. Masoudi).

0378-5173/$ – see front matter © 2012 Elsevier B.V. All rights reserved.
http://dx.doi.org/10.1016/j.ijpharm.2012.04.080

a form of extended Derjaguin–Landau–Vervey–Overbeek (DLVO) theory (Vereda et al., 2008).

Since the introduction of SPIONs in biomedical purposes, many natural and synthetic polymers or molecules were developed as capping agents to prepare required colloidal stability for nanoparticles. Between the coatings, dextran (Hong et al., 2008), poly(ethylene glycol) (PEG) (Acar et al., 2005), chitosan (Zhua et al., 2008), poly(vinyl alcohol) (PVA) (Mahmoudi et al., 2009) and some of their derivatives (Chastellain et al., 2004; Feng et al., 2008; Prencipe et al., 2009; Liu et al., 2011) seem to be more favorable mainly as a result of the biocompatibility and hydrophilicity of these materials.

Several efforts have been devoted to investigate the effect of coating parameters on colloidal stability of SPIONs dispersions. Lozsán et al. (2005) analytically calculated the correspondence of mixing interaction energies between sterically stabilized colloidal particles and other previous models. Viota et al. (2005) looked into the consequence of exploiting poly(acrylic acid) (PAA) adsorbed layer on the stability of suspension. Gómez-Lopera et al. (2006) inspected the stability of magnetite/poly(lactic acid) (PLA) core/shell nanoparticles in the presence and without applied external magnetic field to evaluate the influence of coating shell. Di Marco et al. (2007a) studied the hydrodynamic size evolution of iron oxide nanoparticles coated by two different molecular weights of PEG and amino-alcohol derivatives of glucose at different NaCl concentrations and interpreted the results using the classical DLVO theory. Chanteau et al. (2009) employed citric acid, phosphonate-terminated PEG, and poly(acrylic acid) (PAA) as electrostatic adlayers for maghemite nanoparticles. To ensure that coated nanoparticles can preserve their stability in biological applications, nanoparticles were assessed with respect to changes in concentration, pH and ionic strength of a test solution and finally were evaluated in cell culture medium (DMEM). Barrera et al. (2009) similarly examined PEG silane-coated SPIONs stability at different pHs and ionic strengths and linked their results to DLVO theory. Kim et al. (2010) used CL-PEG as the embedding agent and evaluated stability in terms of function of optical density versus time. They described that weak anchoring of conventional surface modifiers could be annihilated with amphiphilic polymers.

Investigations in the current article are directed to find an answer to the problem about effect of polymer adsorbed layer on colloidal stability and in vivo biodistribution of coated SPIONs as MRI contrast agent. Previously, it has been demonstrated that PEG modified SPIONs exhibit rather long bloodstream circulation time, non-immunogenic and nonantigenic trait and are resistant to protein binding (Hu et al., 2006; Gupta and Gupta, 2005). For these reasons and due to its biocompatibility, highly dynamic motion and extended chain conformation (Wang et al., 2008), PEG is chosen as the capping agent in our study. However, one of the main limitations to take advantages of PEG coated SPIONs dispersions as MRI contrast enhancement agent is weak nanoparticle–polymer bonding which gives rise to poor colloidal stability as a result of polymer desorption.

Here, we synthesized PEG modified nanoparticles using an ultrasonic assisted co-precipitation technique and assessed the colloidal stability through optical density measurements in various pHs and ionic strengths. Furthermore, the uptake of subcutaneously administrated nanoparticles by the lymphatic nodes was detected by in vivo MR imaging of live rats to correlate the stability results of experimental data with their behavior in real biological media.

2. Materials and methods

2.1. Materials

Iron (III) chloride hexahydrate ($FeCl_3{\cdot}6H_2O$), iron (II) chloride tetrahydrate ($FeCl_2{\cdot}4H_2O$), sodium hydroxide (NaOH), hydrochloric acid (HCl, 35 wt.%), nitric acid (HNO_3, 63 wt.%), hydrazine hydrate ($N_2H_4{\cdot}H_2O$, 50 wt.%), sodium chloride (NaCl), potassium ferrocyanide ($K_4Fe(CN)_6{\cdot}3H_2O$), and poly(ethylene glycol) (PEG, M_w = 6000) were all purchased from the Merck (Germany). All the chemical reagents in this work were of analytical grade and used as received without further purification. Deionized distilled water (>18.2 MΩ cm, Milli-Q Academic, Millipore, France) and high purity argon (99.9999%) were also used in experiments.

2.2. Preparation of PEG-coated iron oxide colloidal dispersion

An ex situ manner was employed to synthesis PEG-coated iron oxide nanoparticles as depicted in Fig. 1. First, iron oxide nanoparticles were prepared via an ultrasonic assisted co-precipitation process. 1 mmol (0.198 g) $FeCl_2{\cdot}4H_2O$ and 2 mmol (0.540 g) $FeCl_3{\cdot}6H_2O$ were added into a reactor containing 100 ml deionized H_2O with 200 μl hydrazine hydrate and ultrasonicated (Bandelin SONOPULS HD2200, Germany) for about 30 min under ultra-pure argon atmosphere. Gradually, salt solution temperature was risen to 80 °C using hot-plate apparatus. After reaching the desired temperature, 20 mmol (0.8 g) NaOH was quickly dropped into the solution and sonicated for extra 2 h. Black precipitates of dark suspension were separated magnetically to remove any excess reagents and nonmagnetic components. Subsequently, the nanoparticles were washed for 5 times and dispersed in 50 ml DI

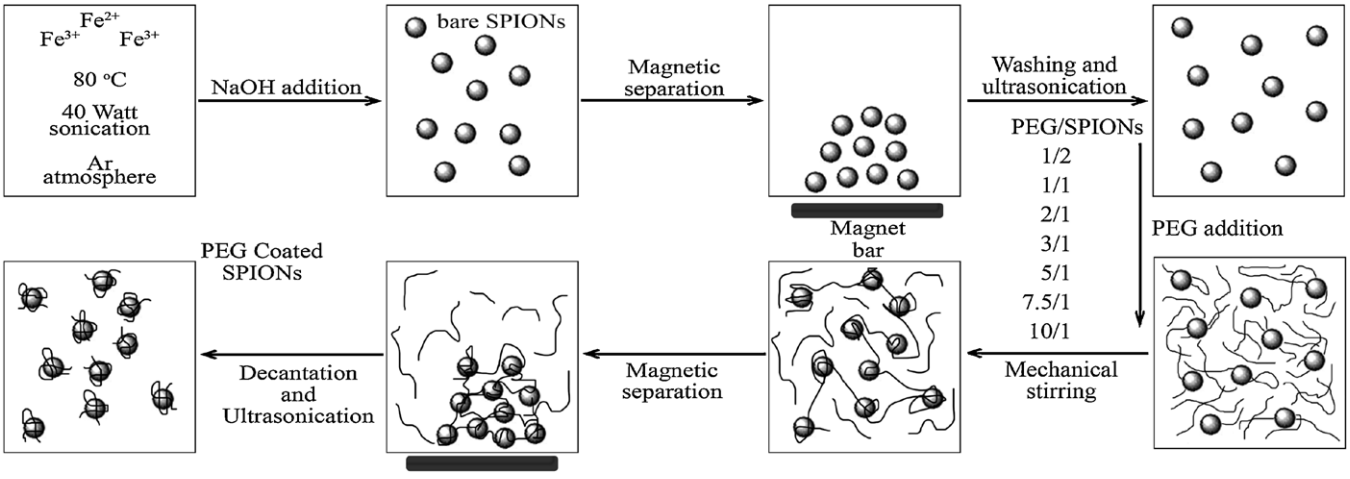

Fig. 1. Sketch map of preparation of PEG-coated nanoparticles (SPIONs).

H_2O by using a bath ultrasonic (Bandelin DT31H, Germany) for 90 min.

Then, coating formation was done by adding PEG solutions to iron oxide suspension in weight ratios of 1/2 to 10/1 PEG/iron oxide and stirring for 24 h via mechanical stirrer at 1000 rpm. At that time, PEG-coated nanoparticles were separated over a strong magnet and the supernatant was decanted. This procedure was repeated several times in company with washing to remove any unanchored polymer. Finally, obtained naoparticles poured into two containers. One portion of separated nanoparticles washed and dried for structural analysis and the other underwent additional sonication step to break any agglomerated clusters formed during magnetic decantation to be used as suspension for colloidal evaluations.

2.3. Characterization methods

The characteristics of the colloidal suspension and involving nanoparticles were examined by different methods. The phase identification of synthesized nanoparticles was performed by X-ray diffraction (XRD, Philips PW 3710, Netherlands) method using a Cu-Kα radiation (λ = 1.5406 Å). Scherrer method was utilized through Philips X'Pert Highscore 1.0d software to determine crystallite size. Fourier transform infrared spectroscopy (FTIR, Bruker Vertex, Germany) was carried out to assess the surface bands of nanoparticles. Consequently, dried nanoparticles were mixed with KBr powder and then were pressed to produce pellets. Nanoparticles size and morphology were investigated by transmission electron microscope (TEM, Philips CM200, Netherlands) and field emission scanning electron microscope (FE-SEM, Hitachi 4160, Japan). Due to propensity of agglomeration, especially in the case of uncoated nanoparticles that resulted in inferior quality of obtained TEM images, bare sample suffered a preparation step of spin coating and freeze drying. After the micrographs were obtained, image analysis was performed by the Clemex Vision PE 4 software. An analysis routine was written to measure the coated nanoparticles size. Hydrodynamic diameter of suspended nanoparticles was determined by dynamic light scattering (DLS, 4700 Malvern Instruments, UK) at 632 nm wavelength laser and a scattering angle of 90° in 0.005 M NaCl solution of pH = 4.7 as electrolyte. Measurements were performed on 0.1 mg [Fe]/l as-prepared dispersions of nanoparticles without any filtration or centrifugation. The results were obtained with theoretical refractive index of magnetite 2.42 (Cornell and Schwertmann, 1996) and analyzed by the cumulant method as intensity distribution curves. The mass of the adsorbed PEG layer on the surface of nanoparticles was measured by thermogravimetric analysis (TGA, Perkin-Elmer TGA7, USA) scanning from room temperature to 700 °C at 10 °C/min heating rate in the atmosphere of N_2. Electrophoresis mobility values of the coated nanoparticles at different pHs were determined via Zetasizer nanosystem (Malvern Instruments, UK). NaOH and HCl dilute solutions were used to adjust the desired pH of aqueous solution. Iron concentration of suspensions was acquired with atomic absorption spectroscopy (AA, Avanta GBC Scientific, USA) of digested samples with boiling HNO_3.

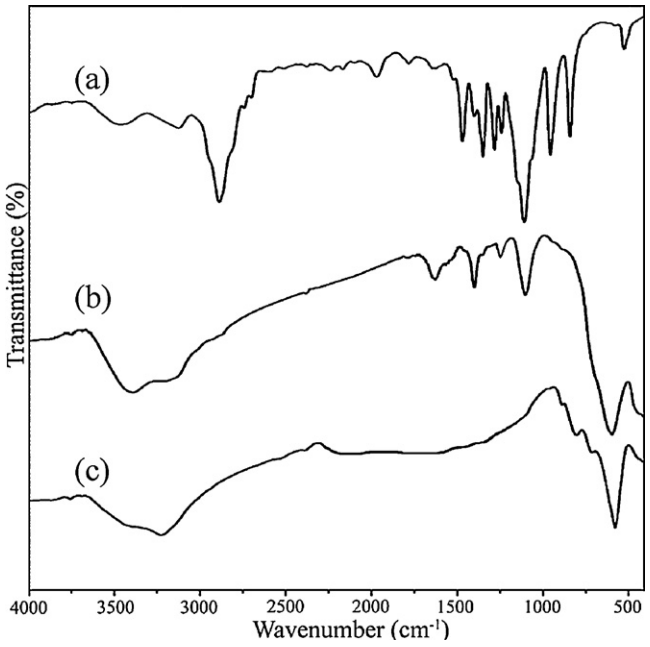

Fig. 3. FTIR spectrum of (a) PEG-6000, (b) PEG-coated (2/1 ratio) and (c) bare iron oxide nanoparticles.

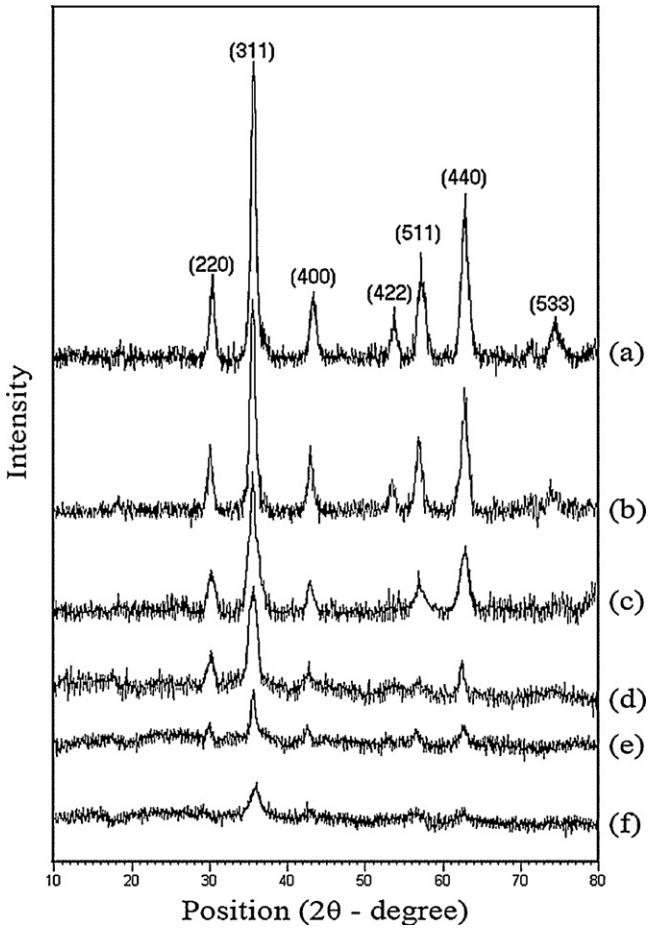

Fig. 2. XRD pattern of (a) bare nanoparticles and PEG/SPIONs weigh rations of (b) 1/2, (c) 1/1, (d) 2/1, (e) 5/1 and (f) 10/1.

Table 1
Size and coating content of nanoparticles at different ratios of PEG/SPIONs.

PEG/SPIONs weight ratio	d_{TEM} (nm)	$d_{hydrodynamic}$ (nm)	Coating percent (%)
0/1 (bare)	4.7 ± 0.9	7.9 ± 1.4	–
1/2	5.3 ± 1.4	12.5 ± 3.7	9.1
1/1	7.1 ± 1.5	15.8 ± 5.3	14.9
2/1	8.9 ± 2.3	24.1 ± 9.2	25
3/1	10.5 ± 3.7	41.6 ± 9.5	41.8
5/1	12.8 ± 5.8	38.7 ± 6.4	53.6
7.5/1	17.9 ± 7.9	56.2 ± 7.0	64.2
10/1	20.6 ± 9.3	63.3 ± 10.9	70.5

2.4. Colloidal stability evaluation

All of the colloidal stability analyses in this research are based on optical absorbance density of the prepared suspensions measured with a UV–Vis double-beam spectrophotometer (Lambda 35 Perkin-Elmer, USA). The stability was studied as a function of pH and ionic strength in terms of NaCl concentration of suspending medium (A) regarding the initial absorbance value (A_0). Besides the neutral condition of pH 7, similar stability measurements were carried out at pH values of 4 and 10 which were prepared by adding HCl and NaOH to solutions, respectively. The NaCl concentration was varied from 10^{-5} M up to 0.1 M in an aqueous solution at pH of 7.

In each experiment, 2 ml of 0.1 mg [Fe]/ml suspension of synthesized nanoparticles was added to 2 ml of the test solution (with different pHs and ionic strengths) and quickly mixed with a microsyringe. Subsequently, the absorbance was recorded at the wavelength of 550 nm through 1 cm light pathway square glass

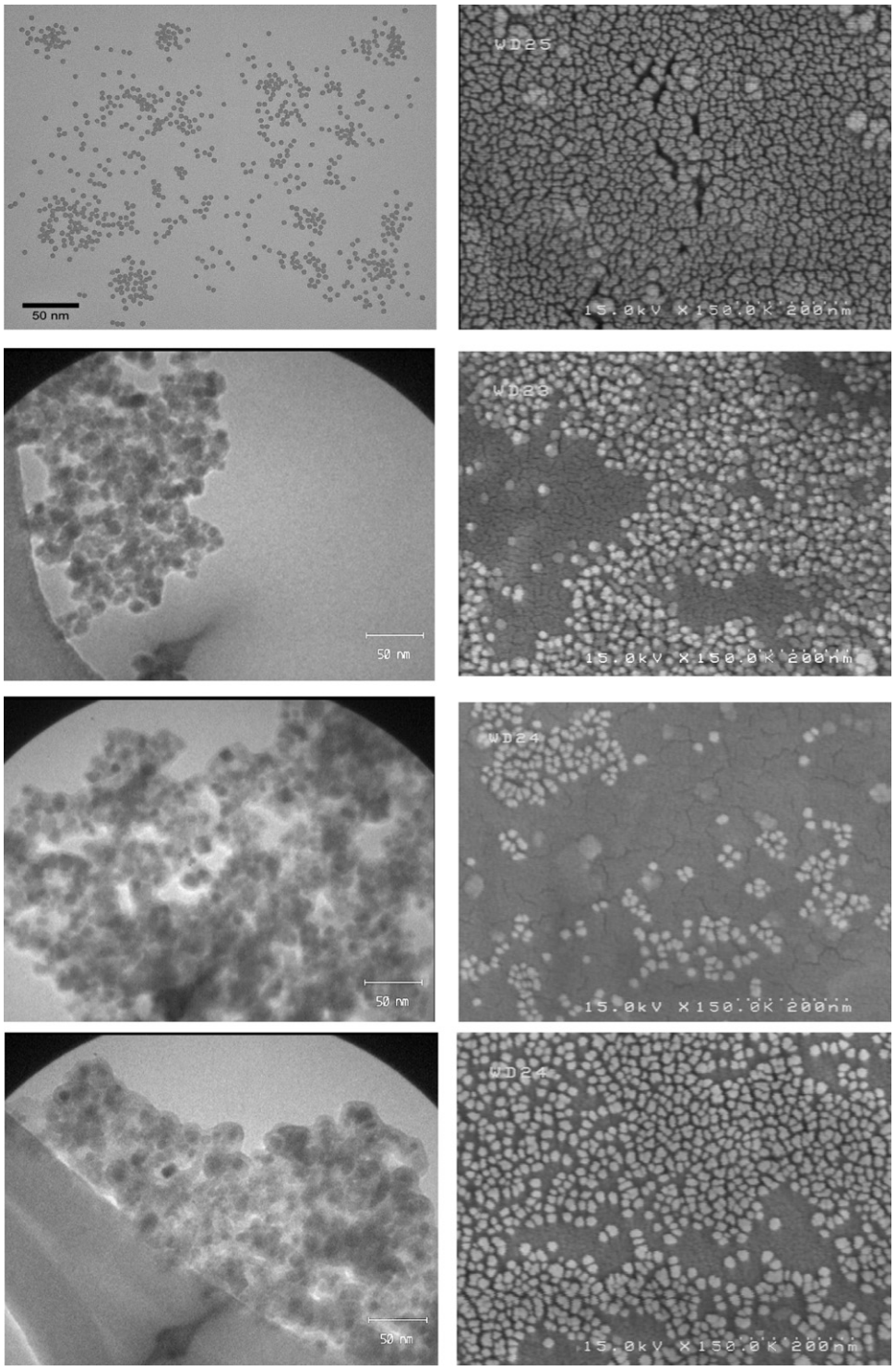

Fig. 4. TEM (left) and SEM (right) micrographs of (a) bare, (b) 2/1, (c) 3/1 and (d) 5/1 PEG/SPIONs weight ratios.

cuvette. An identical cuvette was employed for each sample and no agitation was executed before the measurement. It should be noted that, because of the very different sedimentation rates in various conditions of ionic strength and pH, optical densities were collected at times ranging from 1000 s to 60 days. The obtained optical densities were interpreted to A/A_0 versus time diagrams.

2.5. Prussian blue staining

The uptake of iron oxide nanoparticles by the cells can be probed by Prussian blue staining method. Accordingly, adhesive mouse fibroblast cell line (L929) was obtained from National Cell Bank of Iran (NCBI), Pasteur Institute. The cells were seeded in 24-well plates at 15,000 cells per well in 300 μL of RPMI1640 medium supplemented with 10% fetal bovine serum (FBS) and incubated at 37 °C in 5% CO_2. After 24 h, the cells received 20 μL concentrated 2.2 mg [Fe]/ml suspension. A permanent magnet with a remanence of about 0.7 T attached beneath each well while incubation for second 24 h. After this period the magnet was removed and culture medium/SPIONs complex was replaced with 300 μL fresh RPMI + 10% FBS. The cells were incubated for 72 h. A medium free from nanoparticles was supplied as the negative control sample.

Prussian blue staining was implemented by adding 1:1 volume ratio of 4% potassium ferrocyanide solution and 20% hydrochloric acid to the wells. Any Fe^{3+} ions diffused through the cell react with the ferrocyanide and result in the formation of a bright blue ferric ferrocyanide pigment. After carefully washing each well with DI H_2O, counter staining was achieved by incubating the cells in nucleus fast red solution. The tainted samples were considered under optical microscope.

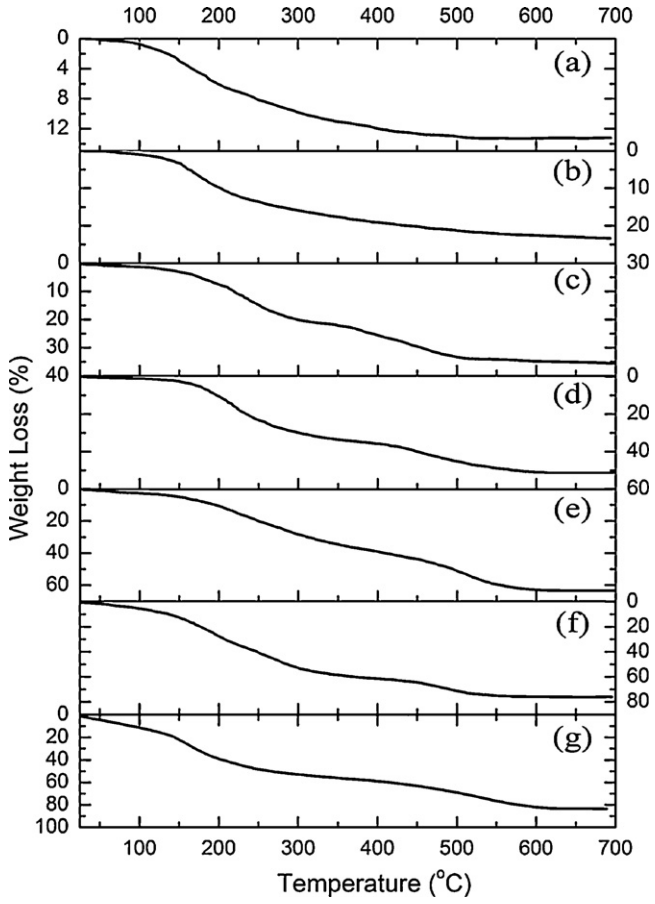

Fig. 5. Weight loss diagrams of PEG-coated Fe_3O_4 at different PEG/SPIONs ratios of (a) 1/2, (b) 1/1, (c) 2/1, (d) 3/1, (e) 5/1, (f) 7.5/1 and (g) 10/1.

2.6. MRI study

Normal Wistar rats underwent MR lymphography to evaluate the drainage ability of the nanoparticles from the injection site and their uptake and subsequent recognition by the lymph nodes macrophage system. All rats were anesthetized before injection of the nanoparticles, using ethyl ether, and before an imaging session with intraperitoneal injection of ketamine and xylazine to achieve longer anesthesia. The experiments involving rats have been carried out in accordance with EU Directive 2010/63/EU.

The colloidal dispersions of SPIONs were subcutaneously injected into the dorsal portion of one front paw of rats with a dose of 0.4 mg Fe/kg body weight. MR imaging was performed 6 h post nanoparticle administration. For MR imaging, the rats were fixed in a supine position. MR studies were performed using a 1.5 T (Signa, GE Medical Systems, Milwaukee, WI, USA) medical system. A head coil was used for MR imaging. The imaging protocol was a fast gradient echo (FGR) T2* in both coronal and axial orientations using following imaging parameters: TR = 350 ms, TE = 8.5 ms, flip angel = 15°, FOV = 25 mm × 25 mm, matrix size = 160 × 160, slice thickness = 2.5 mm, in order to reach appropriate resolution and the most signal to noise ratio (SNR).

3. Results and discussion

3.1. Analysis of nanoparticles

Fig. 2 illustrates the XRD patterns of synthesized nanoparticles. Characteristic peaks exhibited in XRD pattern of all samples are well-matched with the magnetite (Fe_3O_4) diffraction peaks (JCPDS card no. 19-0629) and confirm the inverse spinel structure of nanoparticles. It is clear that the coating material did not affect crystalline structure of magnetite. Nevertheless, it should be noted that the pattern of nanoparticles exposed to higher PEG/SPIONs weight ratios fall to lower intensities (Fig. 2b–f). This may be an indication for greater amount of adsorbed PEG. As amorphous PEG cannot diffract X-ray, intensity weakening of the patterns links to higher PEG absorption.

The presence of PEG layer on nanoparticle surface was more characterized by FTIR spectroscopy as shown in Fig. 3. FTIR spectra of PEG-6000 and unmodified nanoparticles are demonstrated in Fig. 3a and c for comparison. The —C—O—C— ether stretch band and the vibration band (antisymmetric stretch) are appeared in PEG spectrum at 1101.1 cm^{-1} and 1349.4 cm^{-1}, respectively (Gupta and Wells, 2004). Besides, the absorption bands of 1281.3 cm^{-1} and 1468.8 cm^{-1} attribute to the vibration of —CH_2 (Hu et al., 2008) and

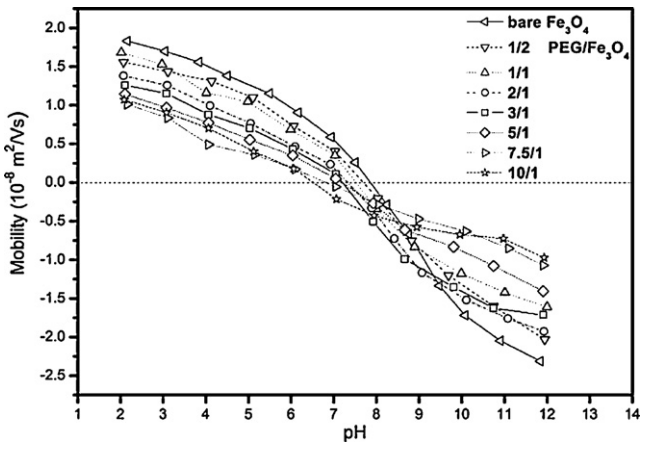

Fig. 6. Electrophoretic mobility of magnetite and coated nanoparticles as a function of pH.

that around 953.2 cm^{-1} corresponds to —CH out-of-plane bending vibration. The transmittance band at 578.1 cm^{-1} of Fig. 3c is the stretching mode of Fe—O in Fe_3O_4 (Ahmadi et al., 2011). The broad peak near 3450 cm^{-1} in both spectra of PEG and iron oxide belongs to attached hydroxyl groups (Gupta and Wells, 2004). The PEG modified nanoparticle spectrum in Fig. 3b comprises the main absorbance of ether stretch band at the 1104.6 cm^{-1} and $—CH_2$ vibrational band at 1260.8 cm^{-1} and 1411.5 cm^{-1}. This spectrum verifies that PEG can be found on the surface of synthesized nanoparticles. However, the characteristic absorbance peaks show a small shift to lower frequencies due to changing the environment of PEG adlayer (Gupta and Wells, 2004). Effective chemical bonding likely leads to such a phenomenon (Basti et al., 2010). Similarly, blue shift of Fe—O vibration of coated nanoparticles to 598.2 cm^{-1} suggests the new band formation between iron oxide surface and PEG coating (Kim et al., 2010).

TEM and SEM micrographs are shown in Fig. 4 and the correlated size of bare and modified nanoparticles is tabulated in Table 1. Fig. 4a reveals that ultrasonic-assisted co-precipitation technique can produce particles with quasi-spherical structure. As it can be seen in this micrograph, the size distribution of bare nanoparticles is fairly narrow that may be attributed to vigorous ultrasonic irradiation. Likewise, adding PEG polymer as the capping agent to the produced nanoparticles did not lead to a significant change in the nanoparticles morphology (Fig. 4b–d). The agglomerated feature of the PEG-coated particles mainly has been originated from drying process of dispersions.

Noteworthy to say that the average crystallite size of bare nanoparticles obtained from XRD analysis (5.8 nm) is in good agreement with real particle size in TEM images (4.7 ± 0.9 nm). This fact implies that Scherrer formula successfully estimates the iron oxide crystallite size in the sub-10 nm scale. Image processing data of other TEM micrographs (not shown) are also presented in Table 1. It is clear that superior PEG/SPIONs ratios leave nanoparticles with greater average particle size. Size increment in PEG modified samples especially at lower ratios up to 2/1, has a magnitude less than

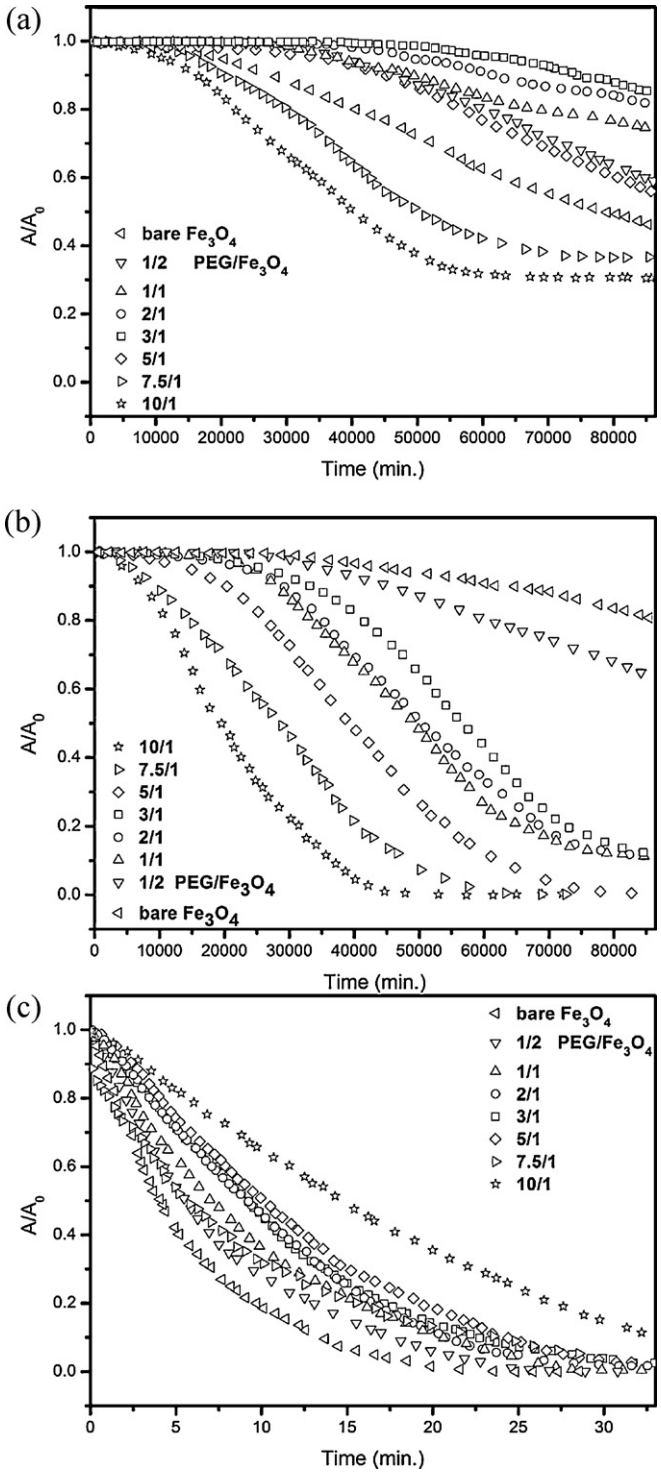

Fig. 7. Relative absorbance as a function of time for synthesized nanoparticles examined at (a) pH = 7, (b) pH = 10 and (c) pH = 4.

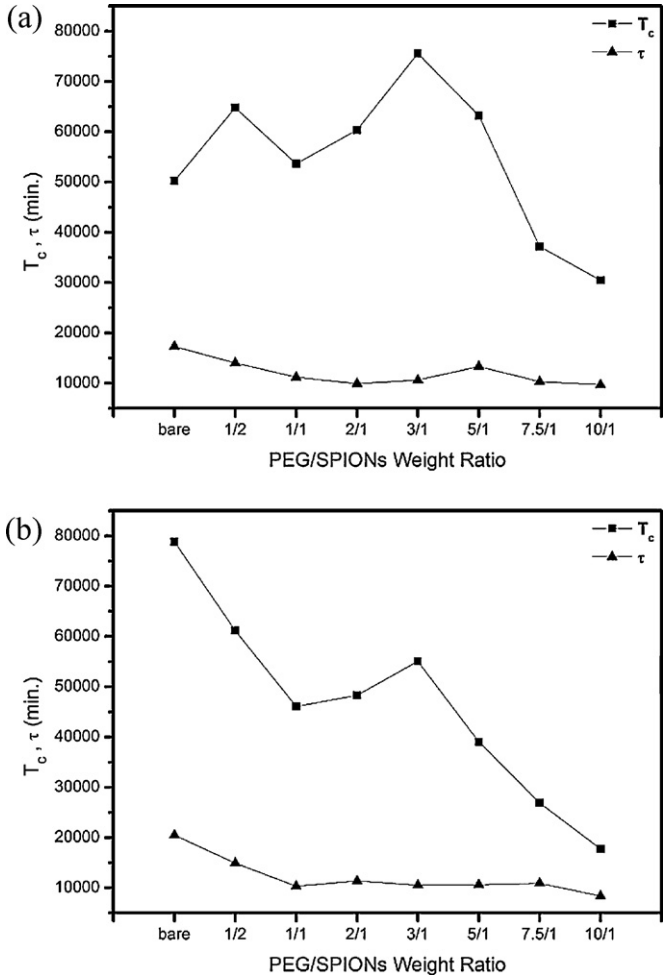

Fig. 8. Time coefficiens (T_c, τ) obtained from sigmoidal equation (1) calculated for experiments at (a) pH = 7 and (b) pH = 10.

magnetite core. This outcome proves the possibility of adlayer formation on a single particle. DLS measurements of nanoparticles (Table 1) clarify a similar conclusion as well. Another interesting subject is the greater size of hydrodynamic diameter compared to the size of TEM images. This may be arisen from "hair layer" model that has been introduced by formation of a hairy layer due to surface molecular chains (Seebergh and Berg, 1995). The other possibility is the induction of surface hydration and electric double layer on the surface of nanoparticles. Di Marco et al. (2007b) believe that the large discrepancy between the crystallite size and hydrodynamic diameters are particularly caused by these effects.

Additionally, the weight loss curves of PEG-coated iron oxide nanoparticles are represented in Fig. 5a–g. In diagrams, the early stage of weight reductions up to about 140–180 °C belongs to the evaporation of water molecules and the second elucidates the PEG decomposition. The latter amounts are quantitatively analyzed and are reflected in Table 1. TGA results indicate that the PEG weight loss fraction w_{PEG} deviates from theoretical value calculated from

$$w_{PEG} = \frac{1}{1 + ((D_0^3 \rho Fe_3O_4)/((D^3 - D_0^3)\rho_{PEG}))} \times 100 \quad (1)$$

where D_0 is Fe_3O_4 crystallite size, D is TEM particle size, $\rho_{Fe_3O_4}$ is the Fe_3O_4 density and ρ_{PEG} is the PEG density. In lower PEG/SPIONs ratio, this deviation is not significant, but greater the PEG ratio the higher the difference. For instance, in the case of 1/2 PEG/SPIONs weight ratio the adsorbed PEG content 9.1% is close to theoretical value of 8. Nonetheless, for 3/1and 5/1 PEG concentrations the formula predicts 68.35% and 80.3% coating efficiency, respectively. These quantities are far from measured data. If coating density defines as the fraction of adsorbed PEG to theoretical value, one can conclude that adding more PEG to embed iron oxide nanoparticles result in inferior PEG compactness. It may be concluded that in higher PEG concentrations, entanglement of PEG interfering chains impedes forming tightly packed shell.

Several formulations in many of previous literatures have been developed to relate electrophoretic mobility to zeta potential of nanoparticles. Many of these formulas require locally planar particle surfaces (like Henry formula) that cannot meet in our coated nanoparticles. On the other hand, misusing the Ohshima equations may lead to some deficiencies (Di Marco et al., 2007a). So, to avoid undesirable errors, the surface charges of synthesized nanoparticles are reported in terms of electrophoretic mobility and are illustrated in Fig. 6.

As pointed out in Fig. 6, the point of zero charge (PZC) gradually moved from 7.8 for unmodified nanoparticles to lower pH values with PEG increment. This is in connection with shielding of surface charge of magnetite nanoparticles by the PEG shell (Illum et al., 2001). The obtained electrophoretic mobility values between ~2 and ~−2.5 ($\times 10^{-8}$ $m^2/V\,s$) assign moderate stability conditions for nanoparticles. In addition, electrophoretic mobility decreases for samples with greater PEG thickness which lessens the electrostatic stability. For this reason, unmodified magnetite nanoparticles have seen with superior mobility and greater PZC value.

3.2. Colloidal stability

3.2.1. The effect of pH

Fig. 7 displays optical absorbance evolution of synthesized nanoparticles as a function of time at different pH values. According to stability theories, absorbance reduction is a consequence of gravitational settling of agglomerated particles (Gómez-Lopera et al., 2006). As Fig. 7a indicates, it is obvious that while certain groups of nanoparticles remained stable in natural and basic conditions over a long period of time for 60 about days, they all completely precipitated at lower pH in about 30 min. Moreover, sedimentation curves of nanoparticles examined under pH 7 and 10 follow a similar trend which is entirely different with the pH 4 trend. Most of the obtained data in colloidal stability measurements especially for evaluations at pH 7 and 10 can be well fitted to the following sigmoidal equation which was previously proposed by Gómez-Lopera to explain the settling features (Gómez-Lopera et al., 2006):

$$\frac{A}{A_0} = \frac{C_1 - C_2}{1 + \exp((t - T_c)/\tau)} + C_2 \quad (2)$$

where T_c and τ are the time coefficients and give detailed information about sedimentation. T_c is a sign of settling commence, whereas, τ inversely corresponds to A/A_0 drop. Then again, results of the tests performed at pH 4 better described with an exponential behavior in the form of

$$\frac{A}{A_0} = C_1' + C_2' \exp\left(-\frac{t}{\tau}\right) \quad (3)$$

which τ is calculated from initial slope (s) of A/A_0 at early times of trial:

$$s = \left.\frac{d(A/A_0)}{dt}\right|_{\tau} \rightarrow 0 = -\frac{C_2'}{\tau} \quad (4)$$

Fig. 8 represents time coefficients for colloidal stability investigations at pH 7 and higher pH of 10. Corresponding results of pH 4 were excluded because relative absorbance values declined rapidly with a quite different formula.

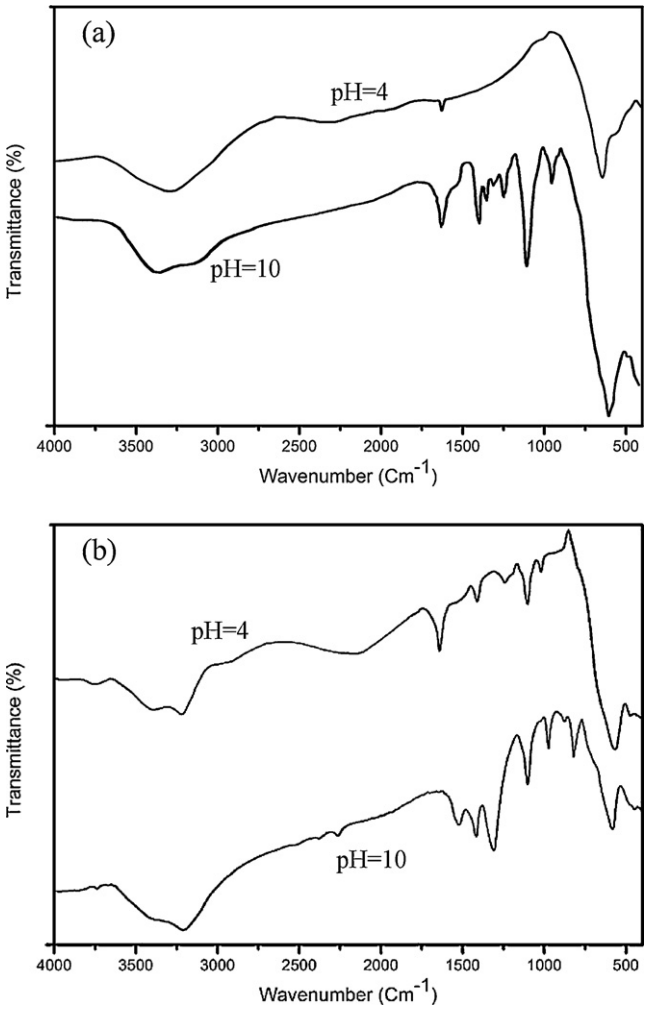

Fig. 9. FTIR spectrum of (a) 2/1 and (b) 10/1 PEG/SPIONs ratio for samples examined at pH 4 and 10.

Figs. 7 and 8 reveal that after 60 days evaluation under neutral conditions, better colloidal stability in starting time of sedimentation and final absorbance values belongs to nanoparticles exposed to up 3/1 PEG/SPIONs weight ratios. However, nanoparticles embedded in higher PEG concentrations of 7.5/1 and 10/1 ratios became unstable with accelerated rate in shorter times and yielded lower absorbance.

It is noticeably observed that at pH 10 that the surface of synthesized nanoparticles was negatively charged (Fig. 6), starting times of deposition, T_c, go along with electrophoretic mobility trait, especially for extreme ratios of PEG/SPIONs. It means that, the higher the electrophoretic mobility the greater the colloidal stability. So, electrostatic repulsion of nanoparticles can effectively hinder particle accumulation at high pH. Higher stability of bare magnetite nanoparticles is an evidence for this fact.

It should be noted that τ time constant was very similar in both pH 7 and 10 for identical samples. In addition, in a determined pH condition this value did not considerably change for samples with intermediate PEG content. This implies that the PEG-coated magnetite nanoparticles settled after a distinct period of evolution, T_c, in a relatively constant speed. Hereafter, once the conditions were prepared, especially attaining critical size of agglomeration, the sedimentation would continue in an independent rate. We believe that sedimentation is governed by particle size and the precipitates may have unique size of agglomerates. We are trying to evaluate this hypothesis by in-line measurement of the agglomerates size.

Another interesting note is lower colloidal stability of nanoparticles with thicker PEG layer at high pH in comparison with pH 7. In contrast, nanoparticles surrounded by more coating material unveiled better stability in acidic solutions. It is noticeable

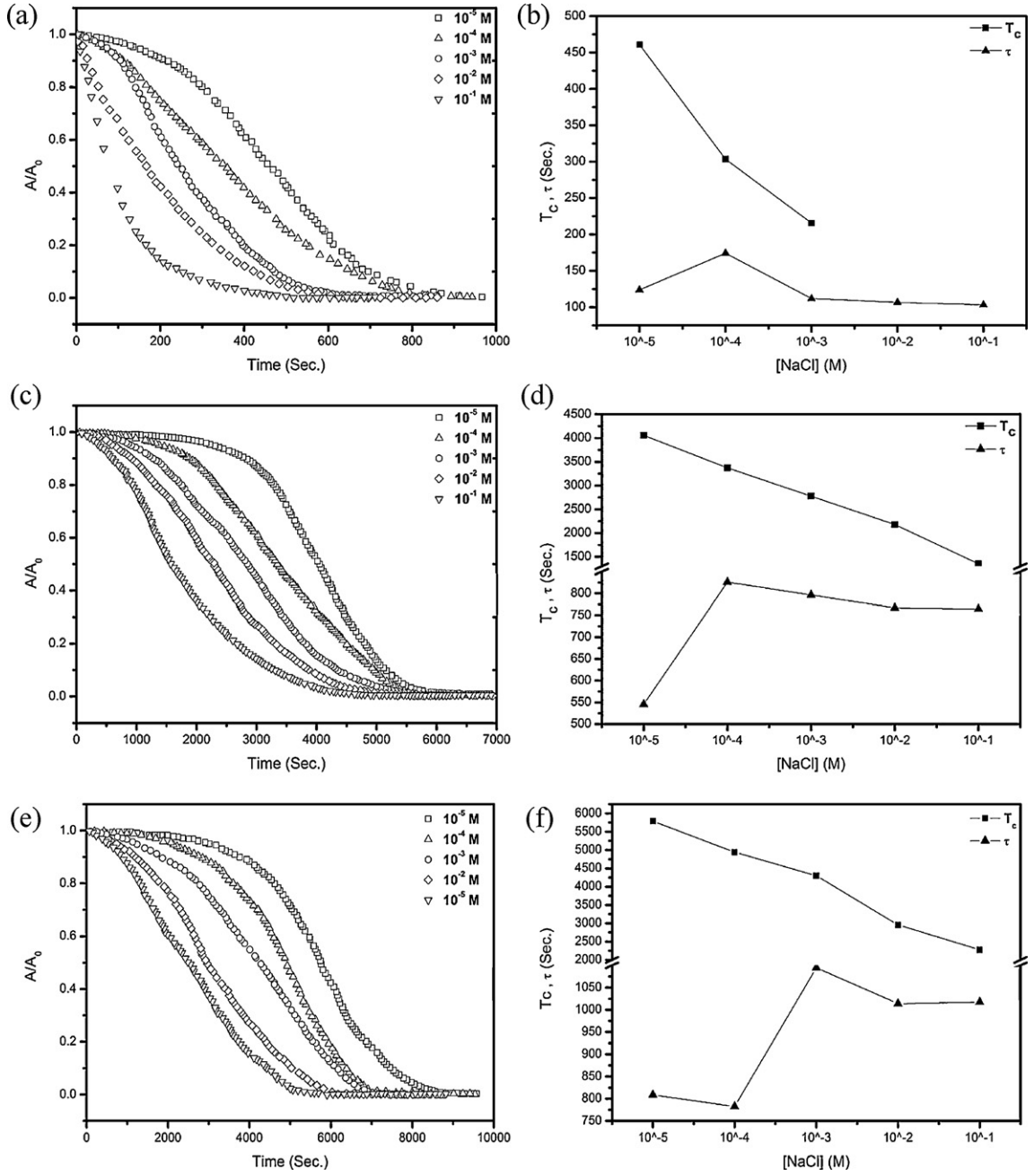

Fig. 10. Relative absorbance (right) and stability time coefficients as a function of time for suspensions examined at various ionic strengths for (a and b) bare, PEG/SPIONs weight ratio of (c and d) 1/2, (e and f) 1/1, (g and h) 2/1, (i and j) 3/1, (k and l) 5/1, (m and n) 7.5/1, (o and p) 10/1.

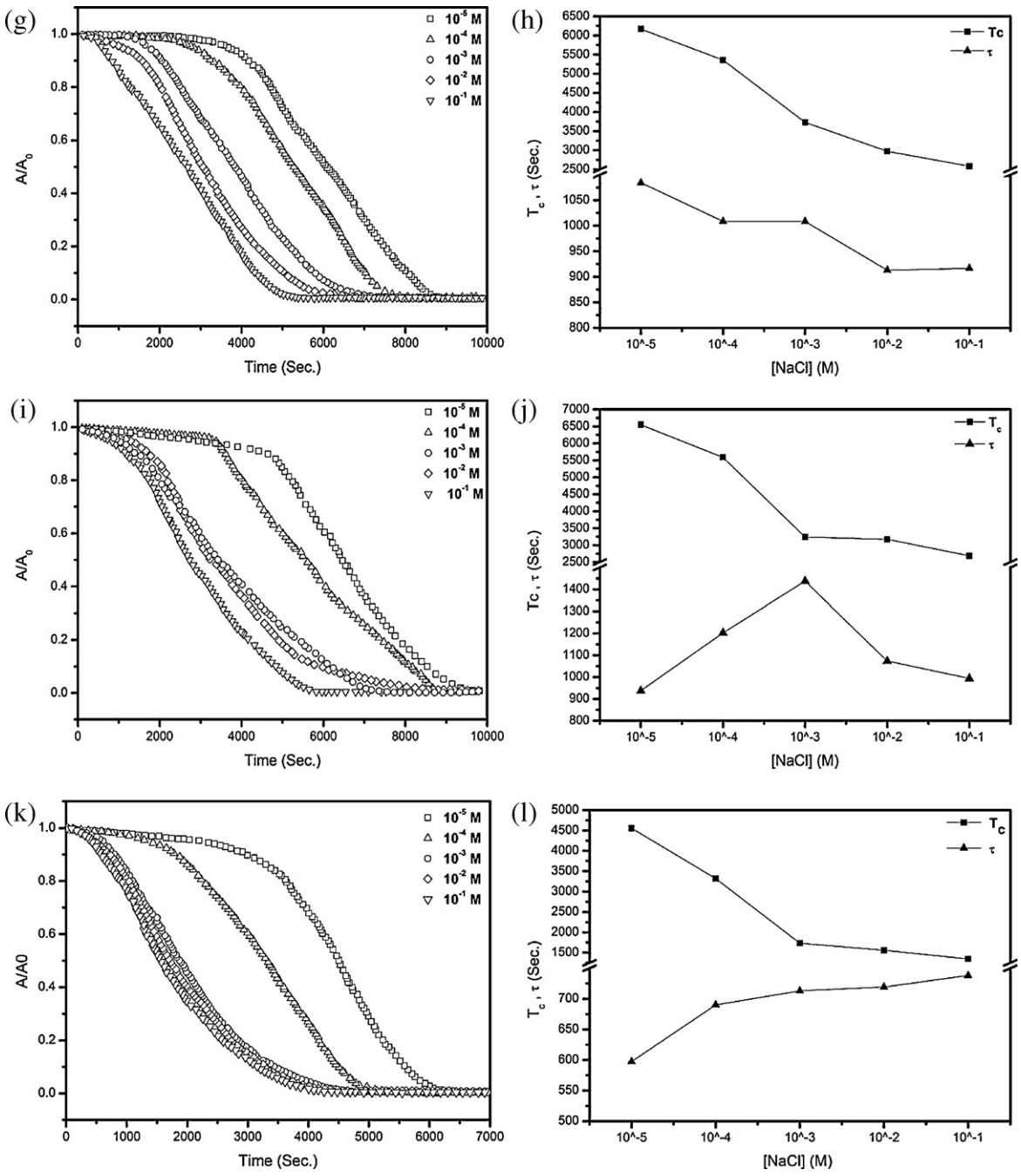

Fig. 10. (*Continued*)

that samples with no coating and those treated with lower weight ratios of PEG suffer from drastic falling of absorbance at low pH. It emphasizes the role of steric repulsion in low pH values and can be described via succeeding studies.

FTIR analysis of nanoparticles that were subjected to acidic and basic conditions (obtained from plateau regions of relative absorbance diagrams) revealed some ambiguities. As clarified in Fig. 9 and compared to Fig. 3, examination under basic conditions did not alter the characteristic bands of PEG coated nanoparticles. As Fig. 9b exhibits, this event was also established for nanoparticles with higher PEG contents tested in acidic solution. But, desorption of thinner shell at pH 4, for instance the case of 2/1 PEG/SPIONs, is recognized from Fig. 9a spectrum in a way that the nanoparticle transmittance bands become similar to uncoated magnetite (Fig. 3c). Additionally, the appeared blue shift in Fe—O bands of nanoparticles tested at pH 4 is anticipated by changing lattice structure, oxidation state or surface environment (Basti et al., 2010). It can be concluded that thicker PEG layers adsorbed from high PEG/SPIONs ratio, better resisted against acidic attack or some intertwined segments has been remained on the nanoparticle surface. Striking speaking, steric hindrance takes effect as the dominant mechanism for colloidal stability at low pH.

3.2.2. The effect of ionic strength

According to stability models, there is a critical point of coagulation (c.c.c.) where at higher concentrations the coagulation rate constant of particles independently changes with solution ionic strength. DLVO theory predicts that by raising salt concentration below c.c.c., the length of electrical double-layer and consequently electrostatic repulsion diminishes.

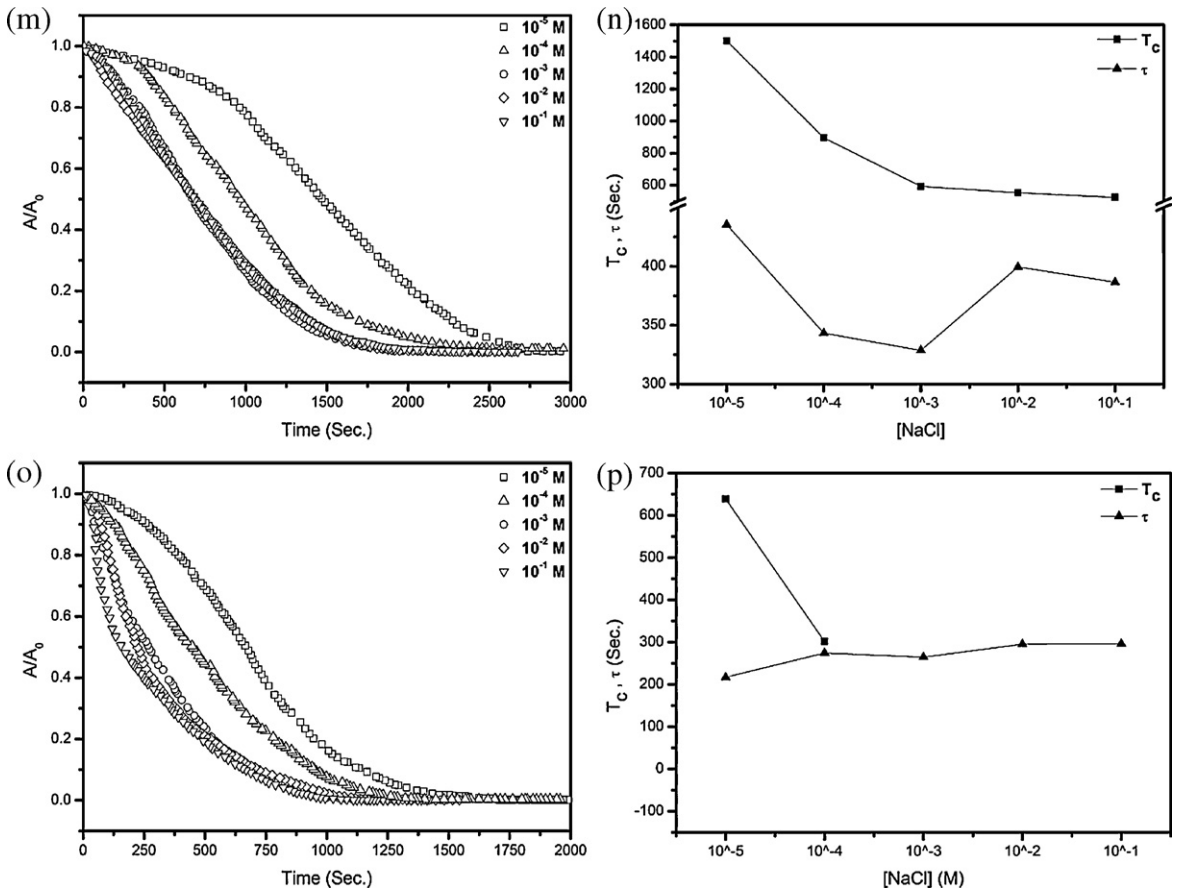

Fig. 10. (*Continued*).

Above the c.c.c., electrostatic repulsion is completely eliminates and aggregation rate constant of particles does not take effect of concentration (Di Marco et al., 2007a). In our current study, colloidal stability measurements were conducted at pH ~ 7 near the point of zero charge (Fig. 6) of the synthesized magnetite nanoparticles. It was done with the aim of suppressing electrostatic repulsion and merely evaluating the electrolyte concentration effect on coating material.

Diagrams of Fig. 10 show time-dependent optical absorbance measurements conducted to assess the role of electrolyte concentration, known as ionic strength, on colloidal stability. Once more, except extreme ionic strength conditions in bare and 10/1 PEG/SPIONs ratio that follow exponential formulation, the other absorbance–time curves lie on a sigmoidal equation.

We observed similarity between τ values in these extreme conditions calculated by both formulations. So, these results are put on view in Fig. 10 (right column). Even though, due to rapid fall of A/A_0 in curves with exponential formula, comparisons between settling commence of two distinct modes of deposition cannot be reasonable. That was so, T_c values exclusively presented for sigmoidal trend and left unfilled for another state.

As Fig. 10 discloses for a sample with specified PEG/SPIONs ratio, T_c increases with decreasing the NaCl concentration of test solution. This fact is observed in all samples. Indeed, precise attention on T_c values divulges that with boosting the coating content as high as 2/1 and 3/1 PEG weight ratios, the starting time of deposition enhances. Higher ratios of PEG not only do not offer the uppermost T_c, but also instigate nanoparticles to settle more readily. Alternatively, ultimate time of examinations which optical absorbance goes to zero is another corroboration of ionic strength effect on colloidal stability. Final deposition time conducts itself in the same direction with T_c. Bare magnetite nanoparticles only take about 600 s in the most diluted salt to be precipitated. This time is further shortened in concentrated solutions. In the case of PEG coated Fe_3O_4 nanoparticles, zero absorbance takes place in much longer times, as extended as 3 h for 2/1 and 3/1 weight ratio. Another time, PEG-coated nanoparticles with greater sizes reach the final stage quicker. Accordingly, in a determined time of evaluation samples with moderate PEG contents had higher relative absorbance.

Then again, samples with intermediate PEG ratio better endure sedimentation and display highest τ. It is apparently discerned that modifying bare Fe_3O_4 nanoparticles with PEG leads to slower sedimentation (longer τ). Contrariwise, adding more PEG content greater than 3/1 weight ratio makes possible faster settling rate. Samples treated with 7.5/1 and 10/1 PEG/SPIONs resist slightly more than unmodified magnetite nanoparticles when exposed to high concentration of NaCl salt. Greater size of these nanoparticles in company with free extended chains of low surface density of PEG adsorbed layer that cause mutual surface bridging, looks to be the main reasons of lesser stability. Moreover, τ time factor signify the critical concentration of coagulation (c.c.c.) approximately above 0.001–0.01 mM where no expressive changes in stability with electrolyte concentration is predictable.

Although, our experiments were performed near the PZC of the nanoparticles that no electrostatic repulsion is proposed, but meaningful variations occur in optical absorbance values with different ionic strength quantities. It can be observed that settling started in shorter times as NaCl concentration enhances and critical concentration of coagulation appeared in much more concentrated solutions. One of the difficulties for this event may derive from the PEG coating. So, FTIR analysis of post treated nanoparticles in NaCl salt solutions was conducted. As Fig. 11 shows, the characteristic

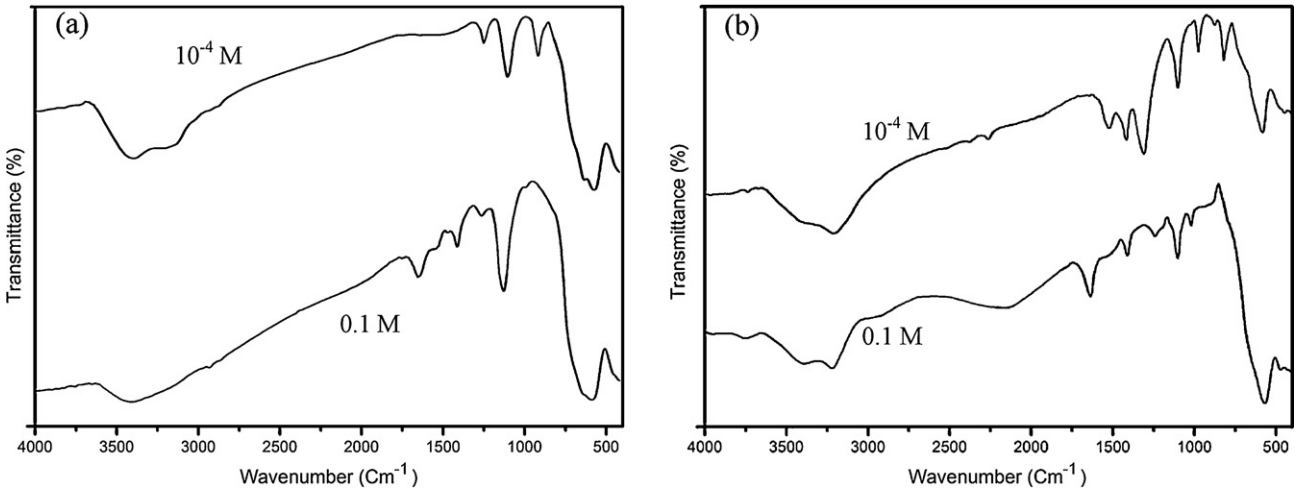

Fig. 11. FTIR spectrum of (a) 2/1, (b) 10/1 PEG/SPIONs ratio for samples examined at 0.1 M and 10^{-4} M NaCl concentrations.

bands of PEG are shifted or are displaced. In spite of this, complete PEG removal cannot be deduced from the spectrum. But, PEG environmental changing is possible. It denotes that steric repulsion is also affected by salt solutions.

3.3. Cell uptake

The stability of different nanoparticles in biological medium and their uptake by cells were evaluated through Prussian blue staining. As can be seen in Fig. 12, bare magnetite nanoparticles quickly agglomerated and deposited on the surface of cells. But it should also be noted that the cells keep their morphology and proliferate in the presence of these big agglomerated clusters of nanoparticles. Since after applying external magnetic field we replaced the culture medium with a fresh one, suspended nanoparticles were poured out. So, these nanoparticles were attached to the bottom of the well and rarely could penetrate the cells. On the other hand, a very noticeable feature of Fig. 12c and d is the presence of green-blue color near the cytoplasm of the cell. Precise scrutiny unfolds that most of the 2/1 PEG/SPIONs nanoparticles were intracellularly dispersed throughout the cytoplasm after 96 h incubation time, while 10/1ratio were attached extracellularly. Cell nuclei were ever free of any nanoparticles. It may be attributed to better colloidal stability and smaller size of particles with lower PEG/SPIONs ratio that make possible their intracellularly drainage.

3.4. MRI results

Accumulation of the nanoparticles in axillary lymph nodes of post contrast MR images for PEG-coated nanoparticles is displayed in Fig. 13. Signal intensity reduction because of nanoparticles accumulation is seen as a ring shape susceptibility artifact in both axillary and brachial lymph nodes in MR images acquired using axial slices. The 3/1 PEG/SPIONs weight ratio sample again better

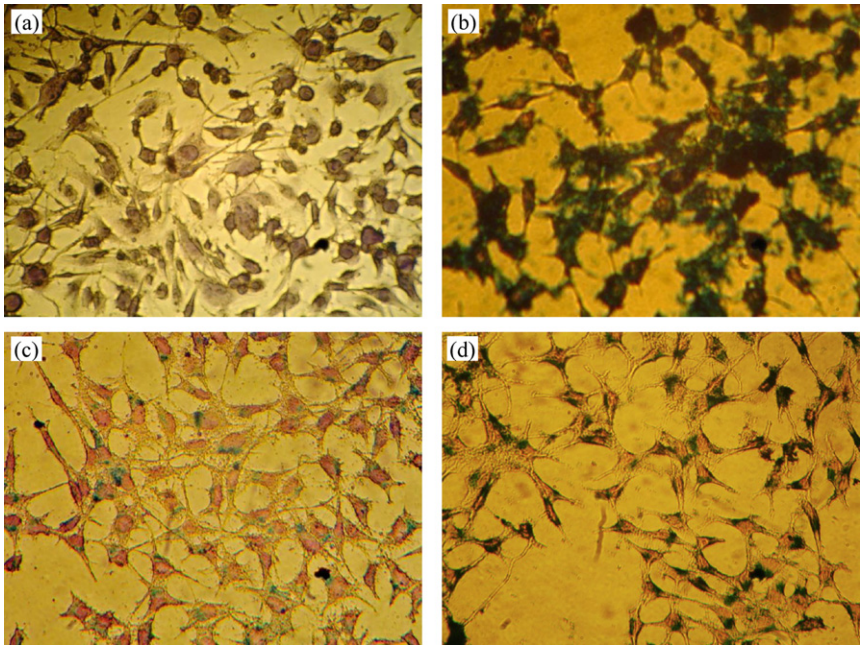

Fig. 12. Follow-up of PEG-coated iron oxide nanoparticles uptake at 96 h with Prussian blue staining for (a) negative control (complete culture medium), (b) bare Fe_3O_4, (c) 3/1, (d) 10/1 PEG/SPIONs weight ratio. Green-blue color denotes iron oxide dispersions and the cells are seen in a pale reddish color. (For interpretation of the references to color in this figure legend, the reader is referred to the web version of the article.)

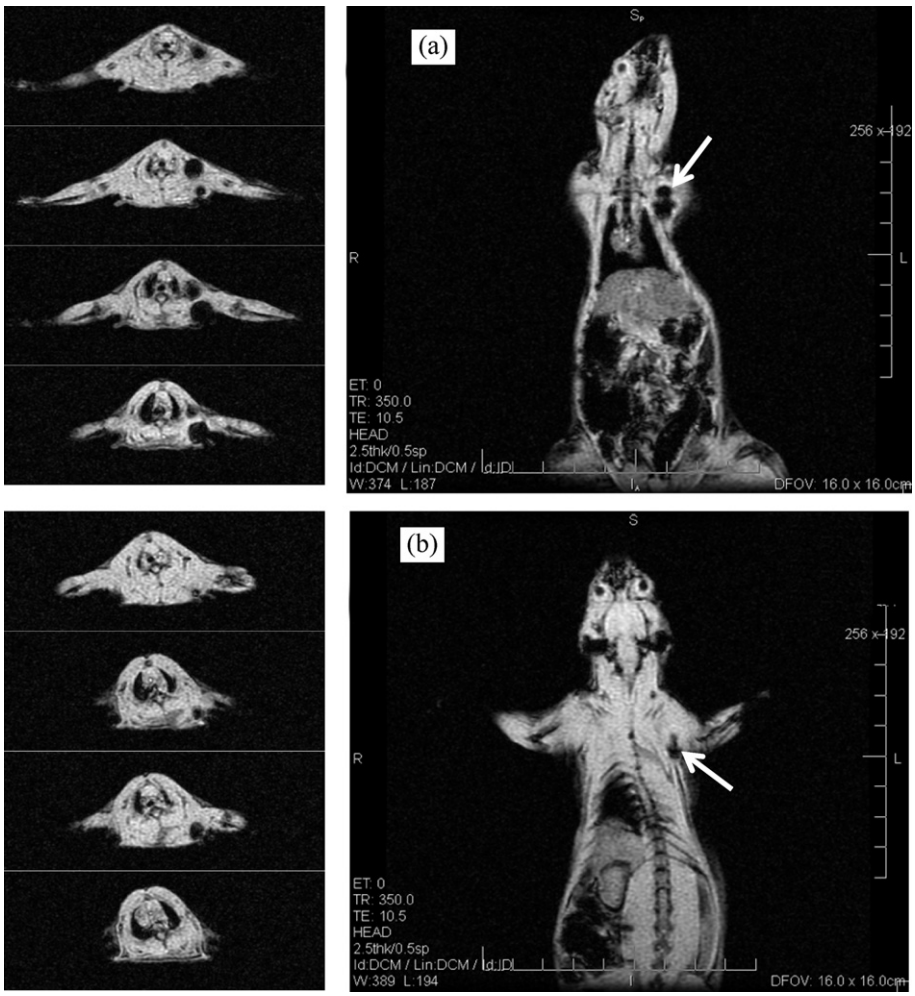

Fig. 13. MR Images of (a) 3/1 and (b) 10/1 PEG-coated SPIONs accumulation in axillary (upper) and brachial (lower dark regions) lymph nodes of rats.

conveyed in bloodstream and appropriately dispersed in lymph nodes, while bigger nanoparticles with higher PEG weight ratio only absorbed by brachial lymph nodes.

4. Conclusions

In summary, ex situ PEG coated nanoparticles were synthesized to be used as potential MRI contrast agent. Colloidal stability evaluation was performed in solutions with different values of pH and ionic strength values to evaluate the behavior of nanoparticles in aqueous phase. It was observed that steric repulsion dominantly hindered van der Waals forces at neutral and low pH conditions. The results showed that an acidic medium can dissolve the capping agent and left the nanoparticles uncoated. So, the dispersion settled quickly in low pH. On the other hand, using higher ionic strength solutions result in faster sedimentation. Among the nanoparticles those exposed to 2/1 to 3/1 PEG/SPIONs ratios further withstand precipitation. We found that samples with moderate coating contents showed superior cell uptake and their intracellular drainage was confirmed. Finally, nanoparticles treated with 3/1 PEG ratio effectively accumulated in axillary and brachial lymph nodes, denoted to the fact that the nanoparticles were stable in bloodstream and remained stealth. Signal reduction study of nanoparticles via MR imaging of lymphatic system revealed that colloidal dispersion of PEG-coated magnetite nanoparticles can be efficiently used as contrast agent.

References

Abdelwahed, W., Degobert, G., Stainmesse, S., Fessi, H., 2006. Freeze-drying of nanoparticles: formulation, process and storage considerations. Adv. Drug Deliv. Rev. 58, 1688–1713.

Acar H.Y.C., Garaas, R.S., Syud, F., Bonitatebus, P., Kulkarni, A.M., 2005. Superparamagnetic nanoparticles stabilized by polymerized PEGylated coatings. J. Magn. Magn. Mater. 293, 1–7.

Ahmadi, R., Malek, M., Madaah Hosseini, H.R., Shokrgozar, M.A., Oghabian, M.A., Masoudi, A., Gu, N., Zhang, Y., 2011. Ultrasonic-assisted synthesis of magnetite based MRI contrast agent using cysteine as the biocapping coating. Mater. Chem. Phys. 131, 170–177.

Barrera, C., Herrera, A.P., Rinaldi, C., 2009. Colloidal dispersions of monodisperse magnetite nanoparticles modified with poly(ethylene glycol). J. Colloid Interface Sci. 329, 107–113.

Basti, H., Tahar, L.B., Smiri, L.S., Herbst, F., Vaulay, M.-J., Chau, F., Ammar, S., Benderbous, S., 2010. Catechol derivatives-coated Fe_3O_4 and γ-Fe_2O_3 nanoparticles as potential MRI contrast agents. J. Colloid Interface Sci. 341, 248–254.

Chanteau, B., Fresnais, J., Berret, J.-F., 2009. Electrosteric enhanced stability of functional sub-10 nm cerium and iron oxide particles in cell culture medium. Langmuir 25, 9064–9070.

Chastellain, M., Petri, A., Hofmann, H., 2004. Particle size investigations of a multistep synthesis of PVA coated superparamagnetic nanoparticles. J. Colloid Interface Sci. 278, 353–360.

Cheong, S.-J., Lee, C.-M., Kim, S.-L., Jeong, H.-J., Kim, E.-M., Park, E.-H., Kim, D.W., Lim, S.T., Sohn, M.-H., 2009. Superparamagnetic iron oxide nanoparticles-loaded chitosan–linoleic acid nanoparticles as an effective hepatocyte-targeted gene delivery system. Int. J. Pharm. 372, 169–176.

Cornell, R.M., Schwertmann, U., 1996. The Iron Oxides: Structure, Properties, Reactions, Occurrence and Uses, 1st ed. VCH, Weinheim, Germany.

de Vicente, J., Delgado, A.V., Plaza, R.C., Durán, J.D.G., Gonzalez-Caballero, F., 2000. Stability of cobalt ferrite colloidal particles. Effect of pH and applied magnetic fields. Langmuir 16, 7954–7961.

Di Marco, M., Guilbert, I., Port, M., Robic, C., Couvreur, P., Dubernet, C., 2007a. Colloidal stability of ultrasmall superparamagnetic iron oxide (USPIO) particles with different coatings. Int. J. Pharm. 331, 197–203.

Di Marco, M., Sadun, C., Port, M., Guilbert, I., Couvreur, P., Dubernet, C., 2007b. Physicochemical characterization of ultrasmall superparamagnetic iron oxide particles (USPIO) for biomedical application as MRI contrast agents. Int. J. Nanomed. 2, 609–622.

Feng, B., Hong, R.Y., Wang, L.S., Guo, L., Li, H.Z., Ding, J., Zheng, Y., Wei, D.G., 2008. Synthesis of Fe_3O_4/APTES/PEG diacid functionalized magnetic nanoparticles for MR imaging. Colloids Surf. A 328, 52–59.

Gómez-Lopera, S.A., Arias, J.L., Gallardo, V., Delgado, Á.V., 2006. Colloidal stability of magnetite/poly(lactic acid) core/shell nanoparticles. Langmuir 22, 2816–2821.

Gupta, A.K., Wells, S., 2004. Surface-modified superparamagnetic nanoparticles for drug delivery: preparation, characterization, and cytotoxicity studies. IEEE Trans. Nanobiosci. 3, 66–73.

Gupta, A.K., Gupta, M., 2005. Synthesis and surface engineering of iron oxide nanoparticles for biomedical applications. Biomaterials 26, 3995–4021.

Handgretinger, R., Lang, P., Schumm, M., Taylor, G., Neu, S., Koscielnak, E., Niethammer, D., Klingebiel, T., 1998. Isolation and transplantation of autologous peripheral $CD34^+$ progenitor cells highly purified by magnetic-activated cell sorting. Bone Marrow Transplant. 21, 987–993.

Hong, R.Y., Feng, B., Chen, L.L., Liu, G.H., Li, H.Z., Zheng, Y., Wei, D.G., 2008. Synthesis, characterization and MRI application of dextran-coated Fe_3O_4 magnetic nanoparticles. Biochem. Eng. J. 42, 290–300.

Hu, F., Neoh, K.G., Cen, L., Kang, E.-T., 2006. Cellular response to magnetic nanoparticles PEGylated via surface-initiated atom transfer radical polymerization. Biomacromolecules 7, 809.

Hu, L., Hach, D., Chaumont, D., Brachais, C.-H., Couvercelle, J.-P., 2008. One step grafting of monomethoxy poly(ethylene glycol) during synthesis of maghemite nanoparticles in aqueous medium. Colloids Surf. A 330, 1–7.

Illum, L., Church, A.E., Butterworth, M.D., Arien, A., Whetstone, J., Davis, S.S., 2001. Development of systems for targeting the regional lymph nodes for diagnostic imaging: in vivo behaviour of colloidal PEG-coated magnetite nanospheres in the rat following interstitial administration. Pharm. Res. 18, 640–645.

Kim, M., Jung, J., Lee, J., Na, K., Park, S., Hyun, J., 2010. Amphiphilic comblike polymers enhance the colloidal stability of Fe_3O_4 nanoparticles. Colloids Surf. B 76, 236–240.

LaConte, E., Nitin, N., Zurkiya, O., Caruntu, D., O'Conno, Ch., 2007. Coating thickness of magnetic iron oxide nanoparticles affects R2 relaxivity. J. Magn. Reson. Imaging 26, 1634–1641.

Laurent, S., Dutz, S., Häfeli, U.O., Mahmoudi, M., 2011. Magnetic fluid hyperthermia: focus on superparamagnetic iron oxide nanoparticles. Adv. Colloid Interface Sci. 166, 8–23.

Ling, Y., Wei, K., Luo, Y., Gao, X., Zhong, S., 2011. Dual docetaxel/superparamagnetic iron oxide loaded nanoparticles for both targeting magnetic resonance imaging and cancer therapy. Biomaterials 32, 7139–7150.

Liu, G., Hong, R.Y., Guo, L., Li, Y.G., Li, H.Z., 2011. Preparation, characterization and MRI application of carboxymethyl dextran coated magnetic nanoparticles. Appl. Surf. Sci. 257, 6711–6717.

Lozsán, A., García-Sucre, M., Urbina-Villalba, G., 2005. Steric interaction between spherical colloidal particles. Phys. Rev. E 72 (061405), 061401–061413.

Ma, H.L., Xu, Y.F., Qi, X.R., Maitani, Y., Nagai, T., 2008. Superparamagnetic iron oxide nanoparticles stabilized by alginate. Pharmacokinetics, tissue distribution, and applications in detecting liver cancers. Int. J. Pharm. 354, 217–226.

Mahmoudi, M., Simchi, A., Imani, M., 2009. Cytotoxicity of uncoated and polyvinyl alcohol coated superparamagnetic iron oxide nanoparticles. J. Phys. Chem. C 113, 9573–9580.

Mahmoudi, M., Sant, S., Wang, B., Laurent, S., Sen, T., 2011. Superparamagnetic iron oxide nanoparticles (SPIONs): development, surface modification and applications in chemotherapy. Adv. Drug Deliv. Rev. 63, 24–46.

Mikhaylova, M., Kim, D.K., Bobrysheva, N., Osmolowsky, M., Semenov, V., Tsakalakos, T., Muhammed, M., 2004. Superparamagnetism of magnetite nanoparticles: dependence on surface modification. Langmuir 20, 2472–2477.

Patel, D., Moon, J.Y., Chang, Y., Kim, T.J., Lee, G.H., 2008. Poly(D,L-lactide-co-glycolide) coated superparamagnetic iron oxide nanoparticles: synthesis, characterization and in vivo study as MRI contrast agent. Colloids Surf. A 313–314, 91–94.

Prencipe, G., Tabakman, S.M., Welsher, K., Liu, Z., Goodwin, A.P., Zhang, L., Henry, J., Dai, H., 2009. PEG branched polymer for functionalization of nanomaterials with ultralong blood circulation. J. Am. Chem. Soc. 131, 4783–4787.

Schweiger, C., Pietzonka, C., Heverhagen, J., Kissel, T., 2011. Novel magnetic iron oxide nanoparticles coated with poly(ethylene imine)-g-poly(ethylene glycol) for potential biomedical application: synthesis, stability, cytotoxicity and MR imaging. Int. J. Pharm. 408, 130–137.

Seebergh, J.E., Berg, J.C., 1995. Evidence of a hairy layer at the surface of polystyrene latex particles. Colloids Surf. A 100, 139–153.

Tadros, T.F., 2007. Colloid Stability: The Role of Surface Forces. Wiley-VCH Verlag, Weinheim.

Theerdhala, S., Bahadur, D., Vitta, S., Perkas, N., Zhong, Z., Gedanken, A., 2010. Sonochemical stabilization of ultrafine colloidal biocompatible magnetite nanoparticles using amino acid, L-arginine, for possible bio applications. Ultrason. Sonochem. 17, 730–737.

Vereda, F., de Vicente, J., Hidalgo-Álvarez, R., 2008. Colloidal characterization of micron-sized rod-like magnetite particles. Colloids Surf. A 319, 122–129.

Viota, J.L., de Vicente, J., Durĭan, J.D.G., Delgado, A.V., 2005. Stabilization of magnetorheological suspensions by polyacrylic acid polymers. J. Colloid Interface Sci. 284, 527–541.

Wang, S., Zhou, Y., Yang, S., Ding, B., 2008. Growing hyperbranched polyglycerols on magnetic nanoparticles to resist nonspecific adsorption of proteins. Colloids Surf. B 67, 122–126.

Yang, C., Rait, A., Pirollo, K.F., Dagata, J.A., Farkas, N., Chang, E.H., 2008. Nanoimmunoliposome delivery of superparamagnetic iron oxide markedly enhances targeting and uptake in human cancer cells in vitro and in vivo. Nanomed.: Nanotechnol. Biol. Med. 4, 318–329.

Zhua, A., Yuan, L., Liao, T., 2008. Suspension of Fe_3O_4 nanoparticles stabilized by chitosan and o-carboxymethylchitosan. Int. J. Pharm. 350, 361–368.